

Article

Cell Viability Study of ZnCuInS/ZnS–TPPS₄ Conjugates against Different Cell Lines as a Promising Fluorescent Probe

Ncediwe Tsolekile ^{1,2,3}, Sundararajan Parani ^{2,3}, Thabang Calvin Lebepe ^{2,3}, Rodney Maluleke ^{2,3},
Vuyelwa Ncapayi ^{2,3}, Mangaka Clara Matoetoe ¹, Sandile Phinda Songca ⁴
and Oluwatobi Samuel Oluwafemi ^{2,3,*}

¹ Department of Chemistry, Cape Peninsula University of Technology, P.O. Box 652, Cape Town 2000, South Africa

² Department of Chemical Sciences, University of Johannesburg, Doornfontein, P.O. Box 17011, Johannesburg 2028, South Africa

³ Centre for Nanomaterials Science Research, University of Johannesburg, Johannesburg 2028, South Africa

⁴ Department of Chemistry, University of KwaZulu-Natal, Private Bag X 54001, Durban 4000, South Africa

* Correspondence: oluwafemi.oluwatobi@gmail.com

Abstract: In the present work, we report a simple synthetic strategy for fabricating ZnCuInS/ZnS–TPPS₄ conjugates and study its cytotoxicity as a promising material for imaging and phototherapy applications. The quaternary QDs were synthesized using eco-friendly materials such as glutathione and water as a solvent, while the anionic 10,15,20-(4-sulphonatophenyl) porphyrin (TPPS₄) was synthesized via the acidification of a meso-tetraphenylporphyrin precursor. Interest in TPPS₄ results from its high-water dispersity, stability, and ability to generate singlet oxygen. Conjugation of ZnCuInS/ZnS QDs with TPPS₄ was performed by titrating porphyrin with different amounts of ZnCuInS/ZnS QDs while keeping all other experimental parameters constant. Comparative analysis of the conjugate to the bare QDs and porphyrin revealed enhanced spectral and photophysical properties. Comparative cytotoxicity assays were performed for TPPS₄ and ZnCuInS/ZnS–TPPS₄ conjugates in BHK21, HeLa, A549, Hek 293 and B16-F10 Nex 2 cell lines using the MTT cell viability assay. The results showed negligible in vitro cytotoxicity indicating the conjugate is an excellent and biocompatible candidate for imaging and phototherapy applications.

Keywords: TPPS₄; ZnCuInS/ZnS QDs; cytotoxicity; TPPS₄–ZnCuInS/ZnS conjugate



Citation: Tsolekile, N.; Parani, S.; Lebepe, T.C.; Maluleke, R.; Ncapayi, V.; Matoetoe, M.C.; Songca, S.P.; Oluwafemi, O.S. Cell Viability Study of ZnCuInS/ZnS–TPPS₄ Conjugates against Different Cell Lines as a Promising Fluorescent Probe.

Organics **2023**, *4*, 126–136. <https://doi.org/10.3390/org4010010>

Academic Editors: Wim Dehaen, Michal Szostak and Huaping Xu

Received: 17 December 2022

Revised: 11 February 2023

Accepted: 9 March 2023

Published: 17 March 2023



Copyright: © 2023 by the authors. Licensee MDPI, Basel, Switzerland. This article is an open access article distributed under the terms and conditions of the Creative Commons Attribution (CC BY) license (<https://creativecommons.org/licenses/by/4.0/>).

1. Introduction

Quantum dots (QDs) are a classical representation of fluorescent semiconductor materials with optoelectronic, shape, and size-dependent properties, which surpasses other nanomaterials [1]. Traditional binary QDs offer enhanced emission and other chemical-physical properties (i.e., tuneable luminescence and bandgap energies), which are distinctive to QDs [2,3]. However, toxic elements used for synthesizing group II–VI (e.g., CdSe, ZnS, etc.)- and group IV–VI (e.g., PbTe, PbS)-based QDs have raised health and environmental challenges. This has resulted in the need to find alternatives to binary QDs. Ternary QDs composed of group I–III–VI elements have addressed many of the binary QDs' shortcomings. The stability, high luminescence, and less toxic nature of ternary QDs have enabled their bio-applications over binary QDs. Although these QDs have exhibited excellent opto-chemical properties, the blue shift observed during their passivation has proved somewhat challenging, particularly for bio-applications, whereby near-infrared emissions are ideal. Yang et al. [4] reported on the organic, multi-step, high-temperature synthesis of luminescent ZnCuInS/ZnS QDs. The group reported increased photoluminescence quantum yield (PLQY) due to the elimination of surface defects. Nonetheless, a blue shift in the absorption and PL band was observed due to quaternary ZnCuInS phase formation due to Zn diffusion into Cu-In-S nanocrystals. In another study, Nady et al.,

synthesized ZnCuInS/ZnS QDs at room temperature [5]. The PL profile observed a blue shift as the Zn²⁺ ion content increased. The observed blue shift was attributed to bandgap widening due to the possible diffusion of Zn²⁺ ions into the crystal structure of the QDs. Zhang et al. [6], also reported a decline in the PL intensity when an excess (up to 70%) of Zn²⁺ was added. The decrease in intensity was attributed to lower levels of Cu²⁺ ions substituted by a large amount of Zn²⁺ ions, or the generation of impurity phases [5,6].

Several mechanisms have been reported to explain the cause of the undesired blue shift in the absorption and PL spectra of ternary QDs. Nonetheless, no consensus has been reached by researchers across different fields. Research has subsequently moved towards developing quaternary QDs (such as ZnCuInS/ZnS QDs) to lower composition toxicities while addressing the blue shifting during ternary core passivation [7].

Porphyrins are cyclic macromolecule dyes commonly used to treat cancer and other non-malignant conditions. They are ideal light harvesters with the ability to generate singlet oxygen, the reactive oxygen species (ROS) required to destroy tumours [8]. The past decade has seen growing development in neutral, anionic, and cationic porphyrins, with the latter showing growing use in bio-applications such as photodynamic therapy and antimicrobial phototherapy [9,10]. Even though porphyrins possess desirable properties such as low dark toxicity, high molecular singlet oxygen generation, and other bio-advantageous properties [11,12], these macrocyclic molecules suffer from several biological drawbacks, including poor bio-distribution, low bio-specificity, and low activity under physiological conditions [13,14]. However, the development of water-soluble anionic porphyrins such as 5,10,15,20-(4-sulphonatophenyl) porphyrin (TPPS₄) has shown valuable electrical and optical features such as a high extinction coefficient in the visible light range, large Stokes displacement, and light stability. Moreover, TPPS₄ has been clinically tested for photodynamic therapy [15–17], highlighting the relevance of this porphyrin in multiple applications.

The growing interest in producing novel multi-functional materials that can be efficiently fine-tuned to act as photosensitizers and perform other unique photochemical roles has prompted the conjugation of porphyrins to nanomaterials. This has resulted in the extension of the application of porphyrin nanomaterial conjugates in fields where porphyrins or QDs alone would prove inadequate. Managa et al. [18] reported the conjugation of meso-tetra(4-carboxyphenyl)porphyrin to graphene carbon quantum dots (GQDs). Cell viability studies performed on the graphene QDs, porphyrin, and the porphyrin–GQD conjugates showed cell viability with dark toxicities of over 90% on MCF-7 breast cancer cells. Martinez et al. [19] investigated the photodynamic inactivation of different bacteria using porphyrin-doped conjugated polymer nanoparticles (CPNs). The group used flow cytometry to study the bacteria–CPN interaction taking advantage of the intrinsic CPN fluorescence and showed that CPNs efficiently bind to the bacterial envelope. The group demonstrated that the porphyrin-doped conjugated polymer nanoparticles were a valuable tool for eliminating multidrug-resistant bacteria.

Herein, we report on the synthesis of quaternary ZnCuInS/ZnS QDs via an eco-friendly method using water as a solvent and biocompatible GSH and sodium citrate as stabilizing agents for dual functionality. Anionic TPPS₄ was then synthesized via the acidification of a tetraphenylporphyrin (TPPH₂) precursor. Following the successful synthesis and characterization of the porphyrin and QDs, a quaternary QDs (ZnCuInS/ZnS QDs) porphyrin (TPPS₄) conjugate was produced. As far as the authors know, no study has evaluated the conjugation of ZnCuInS/ZnS QDs with anionic TPPS₄. The ZnCuInS/ZnS QDs–TPPS₄ conjugate was synthesized by titrating freshly prepared ZnCuInS/ZnS QDs with TPPS₄ via continuous stirring at room temperature. An ideal conjugate system is one where the materials bind in a stoichiometric ratio. However, this is not easily achieved. The binding can be affected by many parameters, such as the multiple conjugation sites on the QDs surface. Therefore, to determine the optimum QD:porphyrin ratio, titration studies were performed whereby the amount of porphyrin in the conjugate was kept constant while the amount of QDs was gradually increased. The spectroscopic and optical properties

of the prepared ZnCuInS/ZnS QDs, TPPS₄, and ZnCuInS/ZnS QDs- TPPS₄ conjugate were characterized using Ultraviolet-Visible spectrophotometry (UV-Vis), Energy Dispersive X-ray Spectroscopy (EDS), Transmission Electron Microscopy (TEM), Photoluminescence (PL) and Fourier-Transform Infrared spectroscopy (FT-IR). Spectral changes in the UV and PL of the ZnCuInS/ZnS-TPPS₄ conjugate were observed and compared to the bare QDs and porphyrin. The changes suggested that surface interaction between the QDs and the porphyrin had occurred. Cytotoxicity analysis of TPPS₄ and the ZnCuInS/ZnS-TPPS₄ conjugate on different cell lines showed insignificant toxicity in both normal and cancer cell lines, with the conjugate showing improved cell survival for HeLa cell lines compared to TPPS₄ alone.

2. Materials and Methods

2.1. Chemicals

Analytical grade copper chloride (CuCl₂), ethanol, propionic acid, indium chloride (InCl₃), sodium citrate dehydrate (Na₃C₆H₅O₇), petroleum ether, calcium chloride, L-glutathione (GSH), sodium sulphide (Na₂S), methanol, zinc acetate dehydrate (Zn(O₂CCH₃)₂(H₂O)₂), thiourea, sodium hydroxide (NaOH), hydrochloric acid (HCl), sodium citrate, pyrrole, sodium bicarbonate, di-sodium hydrogen phosphate buffer, sulphuric acid, methylene blue, 1,3-diphenylbenzofuran, dichloromethane, ethyl acetate, n-hexane, chloroform, acetone, and dimethyl sulfoxide were bought from Sigma Aldrich (Kempton Park, South Africa). Pyrrole was distilled before use, and other chemicals were used without any purification.

2.2. Synthesis of Alloy ZnCuInS QDs and ZnCuInS/ZnS QDs

In a typical reaction adopted from our previous report with modification [20]. Briefly, CuCl₂ (0.011 g, 0.063 mmol), and InCl₃ (0.055 g, 0.25 mmol), were directly mixed in 100 mL of deionized water with continuous magnetic stirring. In the same solution, 20.4 mg Zn(O₂CCH₃)₂(H₂O)₂ (0.093 mmol), 0.294 g Na₃C₆H₅O₇ (1.00 mmol), and 0.09 g GSH (0.29 mmol) were added. The solution pH was modified to 3.60 (using 0.1 M NaOH/0.1 M HCl). Lastly, 25.00 mmol Na₂S stock solution (1.95 g/50 mL) was added to initiate the reaction with continuous magnetic stirring and heating for 45 mins at 95^o C to form ZnCuInS alloy.

ZnCuInS/ZnS QDs was prepared by adding 0.0444 g Zn(O₂CCH₃)₂(H₂O)₂ (0.200 mmol) and 0.015 g CH₄N₂S (0.200 mmol) in-situ into the ZnCuInS solution as ZnS precursors. The reaction was heated for 1 h 20 mins at 95 °C to produce a quaternary ZnCuInS/ZnS core/shell QDs.

2.3. Synthesis and Purification of TPPH₂

The TPPH₂ was synthesized by slowly adding 3.7 mL of freshly purified pyrrole and 5.3 mL of benzaldehyde in 200 mL of boiling propanoic acid at 141 °C. The solution gradually turned dark brown during the addition of benzaldehyde. The solution was refluxed for 30 mins and was allowed to cool to room temperature. The purple product obtained was filtered, the residue was washed with methanol and hot distilled water, and left to dry under the fume hood to get 1.052 g of crude TPPH₂. The column filled with silica gel (60–70 mesh) as the stationary phase and dichloromethane: petroleum ether (3:1) as the mobile phase crude was used to purify TPPH₂.

2.4. Synthesis of Meso-Tetra-(4-Sulfonatophenyl) Porphyrin (TPPS₄)

TPPS₄ was synthesized by modifying the reported standard methods. In short, 0.3952 g of TPPH₂ was added to 10 mL of concentrated sulphuric acid in a round bottom flask. The solution was heated at 141 °C for 6 h with a drying tube (packed with fused CaCl₂). The solution was allowed to cool to room temperature before slowly adding cold distilled water (75 mL). The resulting green residue was washed with 12 mL acetone and allowed to dry. Distilled water (75 mL) was added, followed by Celite, to aid the residue's further

purification. The solution was neutralized using saturated NaHCO_3 to obtain a complete purple solution under an ice bath. The Celite was filtered out from the solution, after which the filtrate was concentrated by adding methanol (~45 mL) while in the ice bath to precipitate the inorganic salts and filtered. The obtained purple residue was rewashed with methanol to produce a solid brown residue. The solid brown residue was dried in the oven and recrystallized with ethanol/methanol (1:5). Finally, the distilled water was used to dissolve the product (TPPS_4), and the pH was adjusted using 0.02 M HCl.

2.5. Conjugation of ZnCuInS/ZnS QDs– TPPS_4

The conjugate was prepared with a ratio of 3:1 (QDs: TPPS_4). Briefly, A solution of ZnCuInS/ZnS QDs (20 mg/20 mL H_2O) was prepared, and then 3 mL of this QDs solution was added to 1 mL of TPPS_4 (0.011 g/100 mL H_2O) followed by magnetic stirring for 1 h. Conjugation of ZnCuInS/ZnS QDs to TPPS_4 was achieved through an esterification process of hydroxyl groups of the free porphyrin and the hydrogen from the carboxylic group of the glutathione (the capping agent for the QDs).

2.6. In Vitro Cytotoxicity of TPPS_4 and ZnCuInS/ZnS– TPPS_4 Conjugate on BHK21, A549, Hek 293, and Hela Cell Lines

MTT (3-(4,5-dimethylthiazol-2-yl)-5-(3-carboxymethoxy-phenyl)-2-(4-sulfophenyl)-2H-tetrazolium) assay protocol was used to determine the in-vitro cytotoxicity of the porphyrin and conjugate on normal kidney fibroblasts (BHK21), cervical cancer (Hela), lung cancer (A549) and kidney cancer (Hek 293) cell lines. Briefly, The 1×10^5 cells/mL of each cell line was incubated in 96-well plates at 37°C overnight, with the subsequent addition of the synthesized TPPS_4 (11.7, 23.4, 46.9, 93.8, 188, and 375 $\mu\text{g}/\text{mL}$) and ZnCuInS/ZnS– TPPS_4 conjugate (24.1, 48.1, 96.3, 193, 385 and 770 $\mu\text{g}/\text{mL}$) at different concentrations. The cells were left to incubate for 4 days, at which point MTT (5.00 μL) was added to the cells. The absorbance values were averaged at 490 nm after 1 h, 2 h, and 4 h incubation periods, and the viability curves were drawn up.

2.7. Characterization

The as-synthesized ZnCuInS/ZnS QDs, TPPS_4 , and ZnCuInS/ZnS QDs– TPPS_4 conjugate were characterized using Ultraviolet-Visible spectrophotometry (UV–Vis) Lambda 25 spectrometer with 1 nm slit width (Perkin Elmer, Beaconsfield, UK); Photoluminescence (PL) (RF-6000, Shimadzu, Kyoto, Japan), Fourier-Transform Infrared spectroscopy (FT-IR) (Spectrum two UATR spectrometer, Perkin Elmer, Beaconsfield, UK), Transmission Electron Microscopy (TEM), and Energy Dispersive Spectroscopy (EDS) (JEOL 2010 operated at 200 kV, Tokyo, Japan).

3. Results

3.1. Characterization of ZnCuInS QDs and ZnCuInS/ZnS QDs

3.1.1. Optical Properties of ZnCuInS QDs and ZnCuInS/ZnS QDs

One-pot synthesis of the ZnCuInS alloy was achieved by intentionally adding Zn^{2+} ions along with the Cu^{2+} and In^{3+} cation precursors into the reaction vessel at the start of the synthesis (Figure 1A). Na_2S was used as a sulphur source in the presence of two stabilizing agents (glutathione and sodium citrate) and water as a solvent to initiate the nucleation process. Herein, GSH and sodium citrate were used to provide sufficient surface binding and control cations (Cu^{2+} and In^{3+}) reactivity with sulphide anions released during the synthesis. The synthesis reaction proceeded at 95°C for 45 min to allow for adequate ZnCuInS growth. Figure 1B gives the typical UV–Vis and PL spectra of the as-synthesized ZnCuInS alloy. The absorption spectra of the ZnCuInS alloy exhibited broad featureless exciton absorption peaks in line with reported studies [21,22]. The corresponding PL exhibited a broad peak at 713 nm and a full-width half maximum (FWHM) of 175 nm. The high FWHM is typical for quaternary QDs and is attributed to excitonic and emission mechanisms produced by point defects [23]. To enhance the luminescence properties

and stability of the alloy, a ZnS shell was grown. The optical properties of the resultant ZnCuInS/ZnS QDs were measured and compared to the ZnCuInS alloy, as depicted in Figure 1B. After passivation with ZnS, the absorption became blue-shifted compared to ZnCuInS alloy, while the PL peak position remained unaltered but with significantly higher intensities. The increase in intensity after the shell formation was further confirmed by the digital images obtained after UV irradiation (Figure 1C).

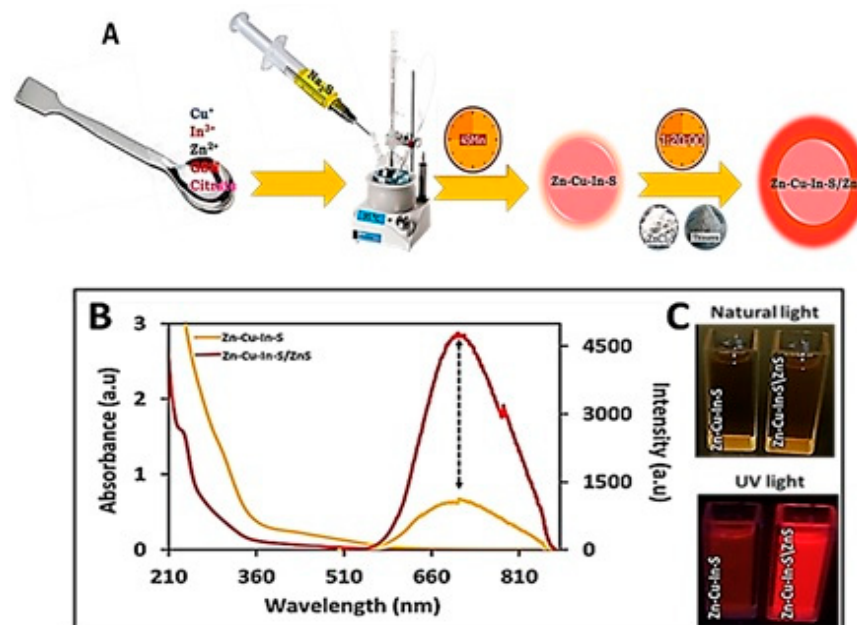


Figure 1. (A) Schematic synthesis of ZnCuInS and ZnCuInS/ZnS. (B) Overlay of absorption and PL of ZnCuInS and ZnCuInS/ZnS. (C) Natural and UV light digital images of ZnCuInS and ZnCuInS/ZnS QDs.

The increase in PL intensities upon ZnS coating was attributed to type 1 band alignment, which results in electron and hole localization, thereby leading to a possible increase in recombination processes. The stable PL peak position (i.e., lack of PL peak blueshift) during ZnS passivation is highly desirable and this could be attributed to the similar ionic radius of 60–62 pm in the four-coordinate structure of the cations involved (In³⁺, Zn²⁺, and Cu⁺ ions) [24,25]. The FWHM of the core/shell ZnCuInS/ZnS QDs was 165 nm. Although the FWHM was reduced compared to the synthesized alloy, it was more significant than binary QDs. Large FWHM are commonly reported in ternary and quaternary Cu/Ag-based QDs and have been attributed to Cu defect state emissions, suggesting that intra-gap levels play a key role in recombination processes [24,26].

3.1.2. Morphology and Structure Characterization of ZnCuInS and ZnCuInS/ZnS QDs

The morphology, elemental, and structural characterization of ZnCuInS and ZnCuInS/ZnS QDs were investigated using TEM, EDS, and FTIR. The TEM micrographs of ZnCuInS (Figure 2A) and ZnCuInS/ZnS QDs (Figure 2C) show that the particles were mono-dispersed and nearly spherical. The ZnCuInS/ZnS QDs further exhibited lattice fringes suggesting highly crystalline nanoparticles. The size distribution curves of ZCIS QDs showed an average particle size of 1.6 ± 0.3 nm (Figure 2B), which increased to 2.7 ± 0.5 nm after ZnS passivation (Figure 2D). The increase in the TEM particle size was attributed to the successful formation of ZCIS/ZnS core/shell QDs.

Figure 3A shows the FTIR spectra of GSH, ZnCuInS, and ZnCuInS/ZnS QDs. The GSH peaks at 3017 cm^{-1} , 3142 cm^{-1} , and 1396 cm^{-1} were assigned to zwitterion $-\text{OOC}-\text{C}-\text{NH}^{3+}$, two NH, and C–O– stretching vibrations, respectively. The GSH spectra showed bands at 1713 cm^{-1} and 1661 cm^{-1} assigned to $-\text{C}=\text{O}$ and the N–H deformation, respectively. The ZnCuInS and ZnCuInS/ZnS QDs spectra showed $-\text{O}-\text{H}$ absorptions at 3248 cm^{-1} and

3326 cm^{-1} , respectively. The ZnCuInS alloy spectra showed an asymmetric $-\text{COO}$ peak at 1605 cm^{-1} and symmetric stretching $-\text{COO}$ peak at 1398 cm^{-1} . After ZnS passivation, the peak at 2318 cm^{-1} was assigned to C–H vibrations while the bands at both 1593 cm^{-1} and 1387 cm^{-1} were assigned to asymmetric and symmetric stretching $-\text{COO}$, respectively. The disappearance of the S–H stretching band in the ZnCuInS/ZnS QDs suggests the capping of GSH through the S–metal bond. The elemental composition of the as-synthesized QDs was confirmed by EDS analysis. The EDS spectrum of the ZnCuInS QDs confirmed the presence of Cu, In, S, and Zn (Figure 3B,C). After the ZnS passivation, a reduction in In and Cu was observed, which suggests some cation exchange (Cu^{2+} , In^{3+} , and Zn^{2+}) on the surface of the QDs during passivation. The increase in S intensity in the quaternary ZnCuInS/ZnS QDs was attributed to the addition of thiourea as a S precursor during passivation.

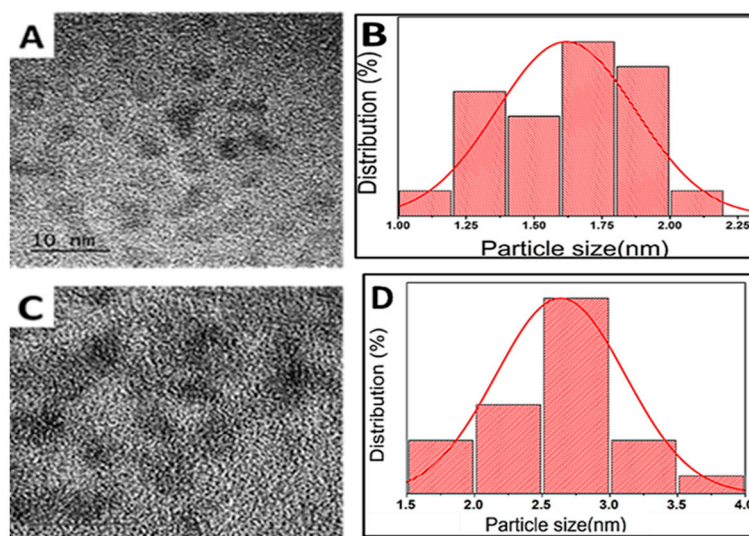


Figure 2. (A) TEM image and (B) size distribution curve of ZnCuInS. (C) TEM image and (D) size distribution curve of ZnCuInS/ZnS QDs.

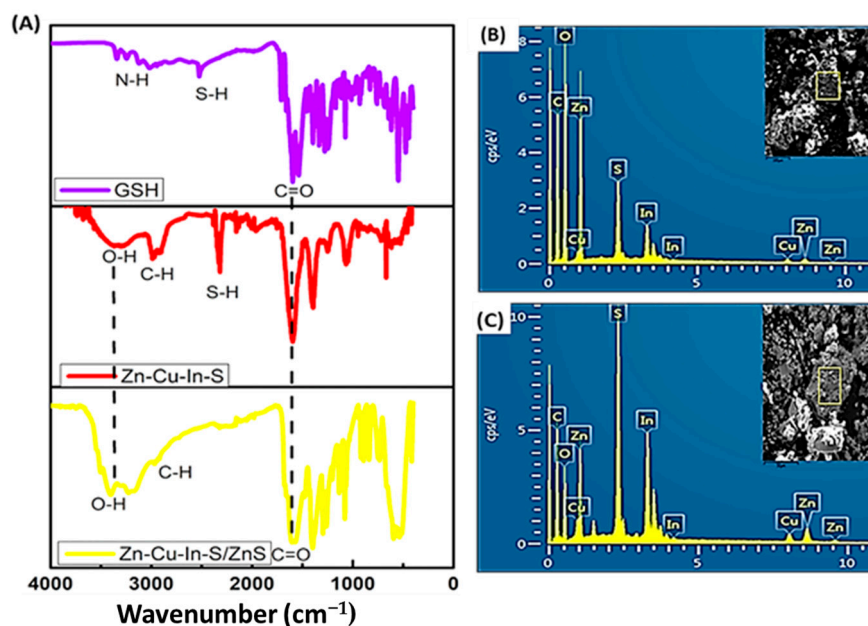


Figure 3. (A) FTIR spectra of GSH, ZnCuInS QDs, and ZnCuInS/ZnS QDs. EDS spectra of (B) Zn-Cu-In-S QDs and (C) ZnCuInS/ZnS QDs (inserts: SEM area of respective material).

3.2. Characterization of TPPS₄

The absorption spectrum of the porphyrin precursor (TPPH₂) is shown in Figure S1 and consists of a Soret band (417 nm) and four Q-bands (514, 549, 589, and 647 nm). After adding H₂SO₄ to TPPH₂ porphyrin, the solution became highly acidic, forming protonated, water-soluble TPPS₄. Figure 4A represents the characteristic absorption peaks of TPPS₄ with a Soret band at 412 nm and four Q-bands (515, 551, 579, and 633 nm) in line with reported studies [15]. Figure 4B shows characteristic FTIR peaks of TPPS₄ with sharp bands at 1118 cm⁻¹ and 1026 cm⁻¹ attributed to S–O str. The C–C stretching vibration absorption peak of the benzene ring and the porphyrin ring was at about 1419 cm⁻¹. The shift in the functional group bands of TPPS₄ from those of TPPH₂ (Figure S1) was used to confirm the structure and successful synthesis of the as-prepared TPPS₄.

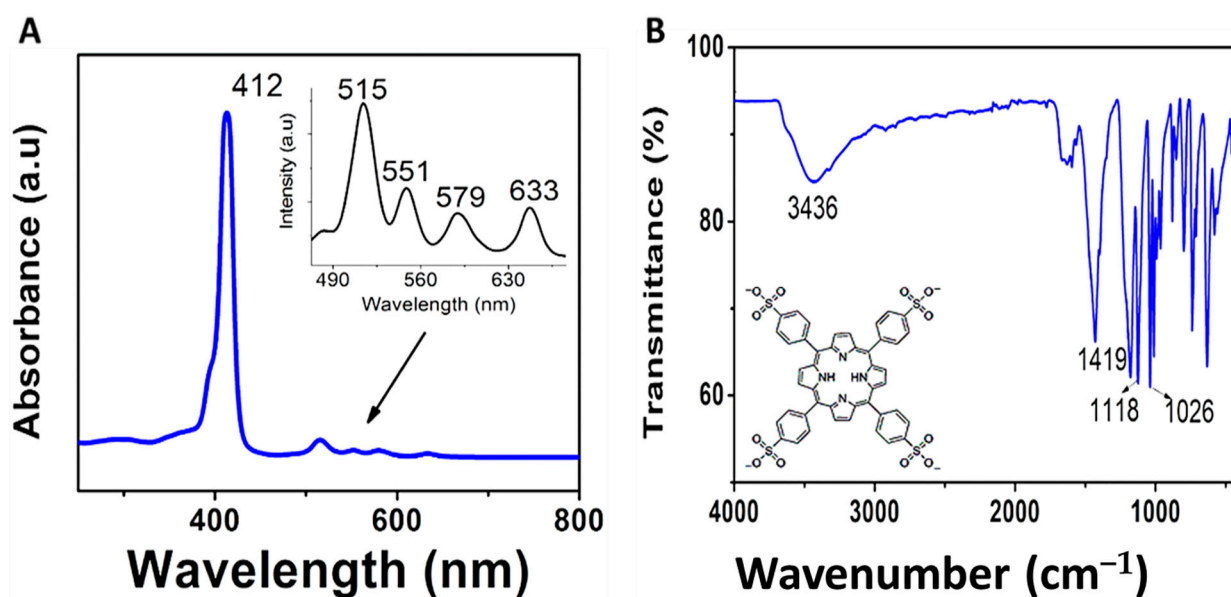


Figure 4. (A) Absorption spectrum (Inset: enlarge spectrum) and (B) FTIR spectrum of TPPS₄.

3.3. Characterization of ZnCuInS/ZnS–TPPS₄ Conjugate

Figure 5A,B show the optical properties of the ZnCuInS/ZnS–TPPS₄ conjugate. During the conjugate preparation, the amount of porphyrin and other experimental variables were kept constant while the amount of QDs was gradually increased. The results show that the conjugate at different QD:porphyrin ratios gave a Soret band (413 nm) but no Q-bands except for the conjugate ratio of 1:1 (Figure 5A,B). This suggests a complete alteration of the absorption of the TPPS₄ in the presence of ZnCuInS/ZnS QDs. Subsequently, a TPPS₄:ZnCuInS/ZnS ratio of 1:1 was used throughout the study. Upon excitation at 535 nm, the conjugate (Figure 5C) exhibited two broad emission bands (645 and 703 nm). At all the ratios examined, the PL peak positions remained relatively constant with a linear reduction in the TPPS₄ emission intensity as the amounts of ZnCuInS/ZnS QDs in the conjugate increased.

The FTIR spectra of TPPS₄ and the ZnCuInS/ZnS–TPPS₄ conjugate are shown in Figure 5D. The band at 3365 cm⁻¹ and 3436 cm⁻¹ of the conjugate and TPPS₄ was assigned to N–H stretching. Compared to the QDs (Figure 3A) and TPPS₄ alone, the IR of the ZnCuInS/ZnS–TPPS₄ conjugate exhibited two sharp peaks at 2923 cm⁻¹ and 2850 cm⁻¹ corresponding to C–H stretching vibrations and O–H stretching vibrations of carboxyl groups, respectively. A shift from the asymmetric and symmetric stretching –COO of the ZnCuInS/ZnS QDs to 1595 cm⁻¹ and 1395 cm⁻¹, respectively, in the conjugate, was observed. The disappearance of TPPS₄ C–C stretching vibration of the benzene ring peak at 1431 cm⁻¹ and the formation of the C–H and O–H stretching vibrations (2923 cm⁻¹ and 2850 cm⁻¹) in the conjugate confirmed the conjugation process.

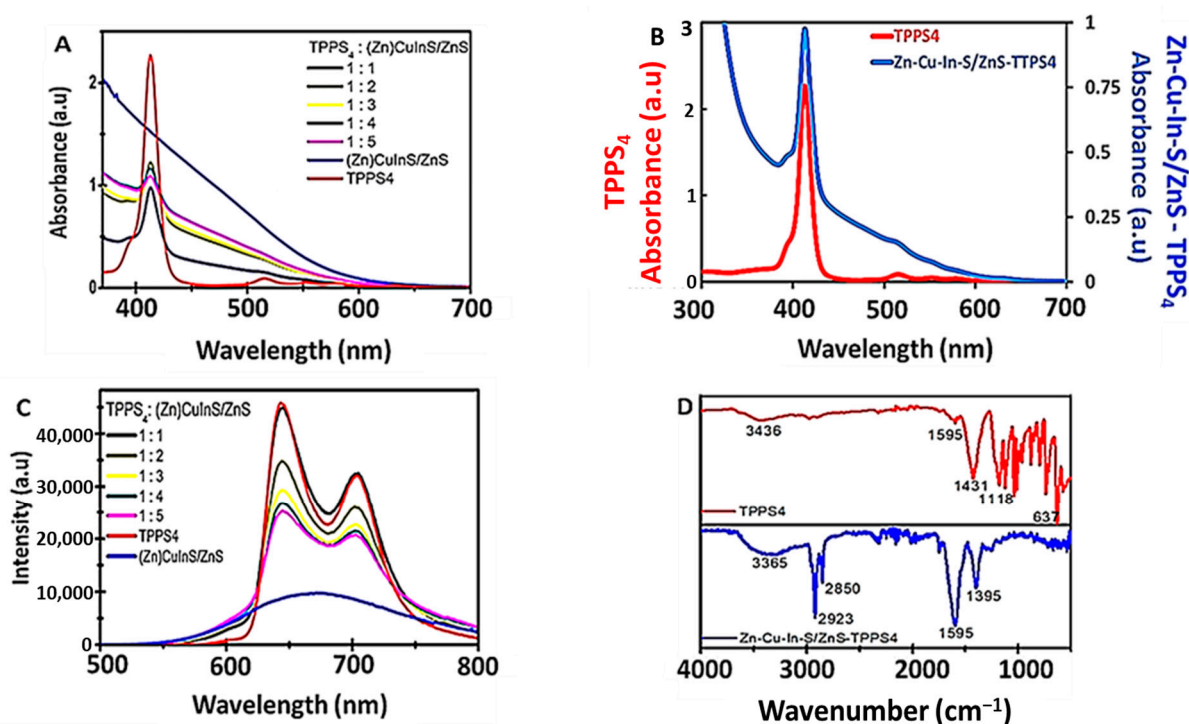


Figure 5. (A) Absorption spectra of TPPS₄, ZnCuInS/ZnS QDs and ZnCuInS/ZnS–TPPS₄ conjugate at different molar ratios of QD:porphyrin ratios. (B) Absorption spectra of ZnCuInS/ZnS–TPPS₄ at TPPS₄: QDs ratio of 1:1. (C) Overlay of the PL spectra of TPPS₄:ZnCuInS/ZnS–TPPS₄. (D) FTIR of TPPS₄ and ZnCuInS/ZnS–TPPS₄ conjugate.

3.4. Cytotoxicity Study of TPPS₄ and ZnCuInS/ZnS–TPPS₄ Conjugate

The biocompatibility of the as-synthesized material (TPPS₄ and ZnCuInS/ZnS–TPPS₄ conjugate) was tested on different cell lines, namely normal kidney fibroblasts (BHK21), cervical cancer (Hela), lung cancer (A549), and kidney cancer (Hek 293) cell lines. The cytotoxicity experiments were measured using a standard methyl thiazole tetrazolium (MTT) assay. The MTT assays were performed on each cell line following exposure of the cells to various concentrations, and the estimate of the cytotoxicity was obtained using the MTT test (data points show the mean and standard deviation, $n = 6$). Figure 6 shows the cytotoxicity of TPPS₄ against the various cell lines. TPPS₄ exhibited excellent cell viability ($\geq 95\%$) against the A549, BHK21, and Hek293 cell lines upon exposure to TPPS₄ up to 375 $\mu\text{g}/\text{mL}$. However, slight toxicity was observed with the Hela cell line compared to the other cancer cell lines.

The MTT assay of the ZnCuInS/ZnS–TPPS₄ conjugate (Figure 7) on different cell lines displayed excellent cell viability ($\geq 97\%$) for all the cancer cell lines (A549, Hek 293, and Hela cells). It is worth noting that the concentrations of the conjugate exposed to the cells were double that of the TPPS₄ porphyrin. This shows that the observed cell viability of the conjugate was not due to the porphyrin only. An increase in cell proliferation was observed for the BHK21 cell line at a level $\geq 193 \mu\text{g}/\text{mL}$ following exposure of the cells to the conjugate. This could be attributed to a possible attack on the cellular nucleus through mutation but further investigation is required. Interestingly, a significant increase in Hela cell survival was observed when the cells were exposed to the ZnCuInS/ZnS–TPPS₄ conjugate compared to TPPS₄ alone. In another study, we reported on a ternary QD–porphyrin conjugate. The results showed that the conjugate possessed high cytotoxicity against THP-1 cells with enhanced localized cell uptake compared to the bare QDs. While confocal imaging of the conjugate indicated effective intracellular penetration [20]. This shows that the conjugate could be used as a selective therapeutic agent against cancer cell lines or as a sensor probe for cancer diagnosis.

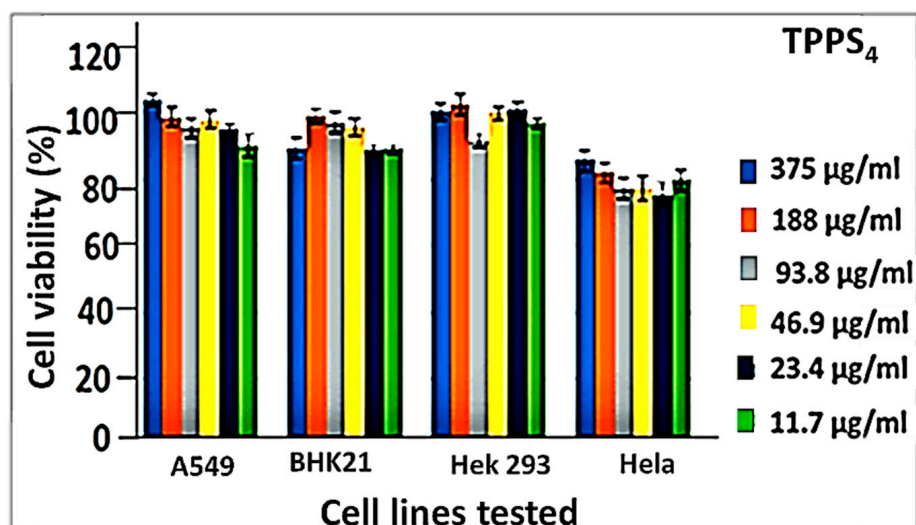


Figure 6. In vitro cytotoxicity of TPPS₄ on different cell lines.

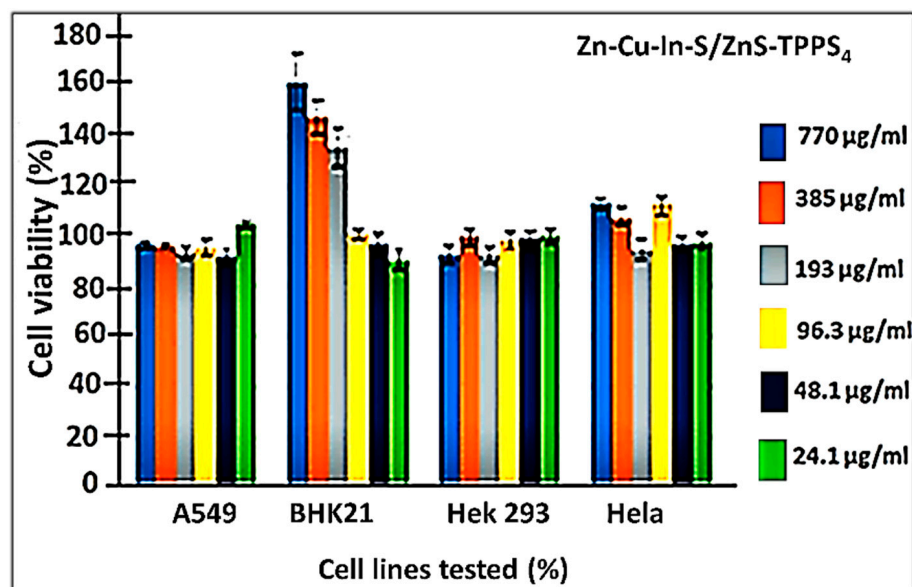


Figure 7. In vitro cytotoxicity of ZnCuInS/ZnS-TPPS₄ conjugate on different cell lines.

4. Conclusions

In summary, highly luminescent and water-soluble ZnCuInS alloy and ZnCuInS/ZnS QDs were synthesized using one-pot synthesis and water as a solvent. Absorption spectra of the synthesized ZnCuInS and ZnCuInS/ZnS QDs exhibited featureless exciton absorption peaks. The PL peak position of the alloy remained unaltered following passivation with ZnS to form ZnCuInS/ZnS QDs. However, the luminescent intensities of ZnCuInS/ZnS QDs increased, accounting for possible type 1 band alignment due to electron and hole localization. The TEM showed that the particles were small, with an average particle diameter of 1.6 ± 0.3 nm and 2.7 ± 0.5 nm for ZCIS alloy and ZCIS/ZnS QDs, respectively. The TPPS₄ exhibited a characteristic Soret band at 413 nm and Q-bands (515, 551, 579, and 633 nm). Following the synthesis of ZnCuInS/ZnS QDs and TPPS₄, we fabricated a ZnCuInS/ZnS-TPPS₄ conjugate for the first time by adding different amounts of QDs to TPPS₄. Spectroscopic studies of the conjugate showed characteristic absorption profiles of ZnCuInS/ZnS and TPPS₄ while maintaining the two broad emission bands (645 and 703 nm) of TPPS₄. Following successful synthesis, cytotoxicity of TPPS₄ and ZnCuInS/ZnS-TPPS₄ conjugate against different cancer and normal cell lines was evaluated via the MTT assay. The TPPS₄ and ZnCuInS/ZnS-TPPS₄ conjugate exhibited low cytotoxicity and good

biocompatibility with both normal and cancer cells, indicating the conjugate is a good and biocompatible candidate for imaging and phototherapy applications.

Supplementary Materials: The following supporting information can be downloaded at: <https://www.mdpi.com/article/10.3390/org4010010/s1>, Figure S1: UV spectra of TPPH₂.

Author Contributions: Conceptualization, N.T., S.P.S. and O.S.O.; methodology, N.T. and S.P.; validation, T.C.L., R.M. and V.N.; formal analysis, N.T. and S.P.; investigation, N.T.; resources, M.C.M. and O.S.O.; writing—original draft preparation, N.T.; writing—review and editing, O.S.O. and S.P.; visualization, T.C.L.; supervision, S.P.S., M.C.M. and O.S.O.; project administration, N.T. and O.S.O.; funding acquisition, N.T. and O.S.O. All authors have read and agreed to the published version of the manuscript.

Funding: This research was funded by the National Research Foundation (NRF), South Africa, under the Nanotechnology Flagship Programme (Grant No. 97983), Competitive Programme for Rated Researchers (Grant Nos. 106060, 129290), Thuthuka (Grant No. 121986), and for equipment-related travel and training (Grant No. 109892).

Data Availability Statement: The data presented in this study are available on request from the corresponding author.

Acknowledgments: The authors would like to thank the Cape Peninsula University of Technology and the University of Johannesburg, South Africa.

Conflicts of Interest: The authors declare no conflict of interest.

References

1. Tsolekile, N.; Parani, S.; Matoetoe, M.C.; Songca, S.P.; Oluwafemi, O.S. Evolution of ternary I–III–VI QDs: Synthesis, characterization, and application. *Nanostruct. Nano-Objects* **2017**, *12*, 46–56. [[CrossRef](#)]
2. Jia, Y.; Wang, H.; Xiang, L.; Liu, X.; Wei, W.; Ma, N.; Sun, D. Tunable emission properties of core-shell ZnCuInS-ZnS quantum dots with enhanced fluorescence intensity. *J. Mater. Sci. Technol.* **2017**, *34*, 942–948. [[CrossRef](#)]
3. Ilaiyaraja, P.; Mocherla, P.S.V.; Srinivasan, T.K.; Sudakar, C. Synthesis of Cu-Deficient and Zn-Graded Cu-In-Zn-S Quantum Dots and Hybrid Inorganic–Organic Nanophosphor Composite for White Light Emission. *ACS Appl. Mater. Interfaces* **2016**, *8*, 12456–12465. [[CrossRef](#)] [[PubMed](#)]
4. Yang, L.; Antanovich, A.; Prudnikau, A.; Taniya, O.S.; Grzhegorzhevskii, K.V.; Zelenovskiy, P.; Terpinskaya, T.; Tang, J.; Artemyev, M. Highly luminescent Zn–Cu–In–S/ZnS core/gradient shell quantum dots prepared from indium sulfide by cation exchange for cell labeling and polymer composites. *Nanotechnology* **2019**, *30*, 395603. [[CrossRef](#)] [[PubMed](#)]
5. Nady, J.E.; Ali, M.; Kamel, O.A.; Ebrahim, S.; Soliman, M. Room temperature synthesis of aqueous ZnCuInS/ZnS quantum dots. *J. Dispers. Sci. Technol.* **2019**, *41*, 1956–1962. [[CrossRef](#)]
6. Zhang, B.; Wang, Y.; Yang, C.; Hu, S.; Gao, Y.; Zhang, Y.; Wang, Y.; Demir, H.V.; Liu, L.; Yong, K.-T. The Composition Effect on the Optical Properties of Aqueous Synthesized Cu–in–S and Zn–Cu–in–S Quantum Dot Nanocrystals. *Phys. Chem. Chem. Phys.* **2015**, *17*, 25133–25141. [[CrossRef](#)]
7. Fang, Z.; Huang, Y.; Cheng, S.; Zhu, Q.; Zhang, W.; Zhao, F.; Huang, G.; Jiang, G.; Li, F. Quaternary alloyed quantum dots with a wide-ranging tunable emission for high color-rendering white light-emitting diodes. *J. Alloys Compd.* **2023**, *932*, 167608. [[CrossRef](#)]
8. Abdulaeva, I.A.; Birin, K.P.; Bessmertnykh-Lemeune, A.; Tsivadze, A.Y.; Gorbunova, Y.G. Heterocycle-appended porphyrins: Synthesis and challenges. *Coord. Chem. Rev.* **2020**, *407*, 213108. [[CrossRef](#)]
9. Moreira, X.; Santos, P.; Faustino, M.A.F.; Raposo, M.M.M.; Costa, S.P.G.; Moura, N.M.M.; Gomes, A.T.P.C.; Almeida, A.; Neves, M.G.P.M.S. An insight into the synthesis of cationic porphyrin-imidazole derivatives and their photodynamic inactivation efficiency against *Escherichia coli*. *Dye. Pigment.* **2020**, *178*, 108330. [[CrossRef](#)]
10. Castriciano, M.A.; Zagami, R.; Casaletto, M.P.; Martel, B.; Trapani, M.; Romeo, A.; Villari, V.; Sciortino, M.T.; Grasso, L.; Guglielmino, S.; et al. Poly(carboxylic acid)-Cyclodextrin/Anionic Porphyrin Finished Fabrics as Photosensitizer Releasers for Antimicrobial Photodynamic Therapy. *Biomacromolecules* **2017**, *18*, 1134–1144. [[CrossRef](#)]
11. Yang, L.; Zhou, J.; Wang, Z.; Li, H.; Wang, K.; Liu, H.; Wu, F. Biocompatible conjugated porphyrin nanoparticles with photodynamic/photothermal performances in cancer therapy. *Dye. Pigment.* **2020**, *182*, 108664. [[CrossRef](#)]
12. Bera, K.; Maiti, S.; Maity, M.; Mandal, C.; Maiti, N.C. Porphyrin-Gold Nanomaterial for Efficient Drug Delivery to Cancerous Cells. *ACS Omega* **2018**, *3*, 4602–4619. [[CrossRef](#)]
13. Kyropoulou, M.; DiLeone, S.; Lanzilotto, A.; Constable, E.C.; Housecroft, C.E.; Meier, W.P.; Cornelia, G. Porphyrin Containing Polymersomes with Enhanced ROS Generation Efficiency: In Vitro Evaluation. *Macromol. Biosci.* **2020**, *20*, 1900291–1900300. [[CrossRef](#)]

14. Rojkiewicz, M.; Kuś, P.; Kozub, P.; Kempa, M. The synthesis of new potential photosensitizers. *Dye. Pigment.* **2013**, *99*, 627–635. [[CrossRef](#)]
15. Chen, J.; Ma, Q.; Hu, X.; Gao, Y.; Yan, X.; Qin, D.; Lu, X. Design of a novel naked-eye and turn-on fluorescence sensor based on the 5,10,15,20-(4-sulphonatophenyl) porphyrin (TPPS4)-Hg²⁺ system: Monitoring of glutathione (GSH) in real samples and DFT calculation. *Sens. Actuators B Chem.* **2018**, *254*, 475–482. [[CrossRef](#)]
16. Parra, G.G.; Ferreira, L.P.; Gonçalves, P.J.; Sizova, S.V.; Oleinikov, V.A.; Morozov, V.N.; Kuzmin, V.A.; Borissevitch, I.E. Stimulation of Cysteine-Coated CdSe/ZnS Quantum Dot Luminescence by meso-Tetrakis (p-sulfonato-phenyl) Porphyrin. *Nanoscale Res. Lett.* **2018**, *13*, 40. [[CrossRef](#)]
17. Kou, J.; Dou, D.; Yang, L. Porphyrin photosensitizers in photodynamic therapy and its applications. *Oncotarget* **2017**, *8*, 81591–81603. [[CrossRef](#)] [[PubMed](#)]
18. Managa, M.; Ngoy, B.P.; Nyokong, T. Photophysical properties and photodynamic therapy activity of a meso-tetra(4-carboxyphenyl)porphyrin tetramethyl ester-graphene quantum dot conjugate. *New J. Chem.* **2019**, *43*, 4518–4524. [[CrossRef](#)]
19. Martínez, S.R.; Ibarra, L.E.; Ponzio, R.A.; Forcone, M.V.; Wendel, A.B.; Chesta, C.; Spesia, M.B.; Palacios, R.E. Photodynamic inactivation of ESKAPE group bacterial pathogens in planktonic and biofilm cultures using metallated porphyrin-doped conjugated polymer nanoparticles. *ACS Infect. Dis.* **2020**, *6*, 2202–2213. [[CrossRef](#)]
20. Tsolekile, N.; Nahle, S.; Zikalala, N.; Parani, S.; Sakho, E.H.M.; Joubert, O.; Matoetoe, M.C.; Songca, S.P.; Oluwafemi, O.S. Cytotoxicity, fluorescence tagging and gene-expression study of CuInS/ZnS QDS-Meso (hydroxyphenyl) porphyrin conjugate against human monocytic leukemia cells. *Sci. Rep.* **2020**, *10*, 4936. [[CrossRef](#)]
21. Yue, L.; Rao, H.; Du, J.; Pan, Z.; Yu, J.; Zhong, X. Comparative advantages of Zn-Cu-In-S alloy QDs in the construction of quantum dot-sensitized solar cells. *RSC Adv.* **2018**, *8*, 3637–3645. [[CrossRef](#)] [[PubMed](#)]
22. Guo, W.; Tu, Y.; Dong, C.; Zhang, B.; Hu, C.; Chang, J. Synthesis of Zn-Cu-In-S/ZnS Core/Shell Quantum Dots with Inhibited Blue-Shift Photoluminescence and Applications for Tumor Targeted Bioimaging. *Theranostics* **2013**, *3*, 99–108. [[CrossRef](#)] [[PubMed](#)]
23. Lin, W.; Huang, Y.; Lee, T.; Lin, P.; Chung, S. High color rendering index of ZCIS quantum dots-based white light-emitting diodes. *NanoSci. + Eng.* **2020**, *104*, 261106.
24. Jia, Y.; Wang, H.; Yan, Z.; Deng, L.; Dong, H. RSC Advances A facile method for the synthesis of CuInS₂-ZnS quantum dots with tunable photoluminescent. *RSC Adv.* **2016**, *6*, 93303–93308. [[CrossRef](#)]
25. Park, J.; Kim, S.-W. CuInS₂/ZnS core/shell quantum dots by cation exchange and their blue-shifted photoluminescence. *J. Mater. Chem.* **2011**, *21*, 3745–3750. [[CrossRef](#)]
26. Jawhar, N.N.; Soheyli, E.; Yazici, A.F.; Mutlugun, E.; Sahraei, R. Preparation of highly emissive and reproducible Cu-In-S/ZnS core/shell quantum dots with a mid-gap emission character. *J. Alloys Compd.* **2020**, *824*, 153906. [[CrossRef](#)]

Disclaimer/Publisher's Note: The statements, opinions and data contained in all publications are solely those of the individual author(s) and contributor(s) and not of MDPI and/or the editor(s). MDPI and/or the editor(s) disclaim responsibility for any injury to people or property resulting from any ideas, methods, instructions or products referred to in the content.